Preprints of the 19th World Congress
The International Federation of Automatic Control
Cape Town, South Africa. August 24-29, 2014

Active Control of Aerodynamic Surfaces for Ride Control in Sport Vehicles

Matteo Corno * **Stefano Bottelli** * **Mara Tanelli** * **Cristiano Spelta** **
Sergio M. Savaresi *

* *Dipartimento di Elettronica Informazione e Bioingegneria, Politecnico di Milano, piazza Leonardo da Vinci, 20133 Milano.*
** *Dipartimento di Ingegneria dell'Informazione e metodi Matematici, Universita' degli Studi di Bergamo, Dalmine (BG)*

Abstract: This work investigates the use of Active Aerodynamic Surfaces (AAS) to enhance ride comfort in sport vehicles. Four AAS's generate lift forces that control the vertical acceleration of the sprung mass without negatively affecting the unsprung mass. It is shown that the AAS system can overcome the trade-off between comfort and road holding. In this work a preliminary analysis of the control system is presented along with a mechatronic feasibility analysis. The required controller bandwidth, airfoils size and power requirements are analyzed in simulation. The system is validated on a complete vehicle model showing improvements of the order of 30% in ride comfort with no negative effects on road-holding at high speed.

Keywords: Vehicle dynamics control, suspension control, active aerodynamics surfaces.

1. INTRODUCTION AND MOTIVATION

Although lately the main focus of many automotive manufacturers is efficiency; automakers continuously strive for vehicles that are safe and pleasurable to drive.

Vehicle dynamics control (VDC) systems are a means to characterize the handling and comfort as well as increasing energy-efficiency and passengers' safety. VDC is increasingly becoming a brand-defining feature. In the past decade numerous VDC systems have been brought to the market (*e.g.*, ABS, ESC, EBD, and many others - see for example Corno et al. (2012) and references cited therein). These systems influence the dynamic behavior of the vehicle relying on different actuators: active brakes (Todeschini et al. (2014)), (semi-)active suspensions (Savaresi et al. (2010); Hong et al. (2002)) and assisted or fully active steering systems.

Advances in mechatronics are making new actuators available; active Aerodynamic Surfaces are an example. The goal of this paper is to investigate the potentials of genuine closed-loop active aerodynamic control for vehicle comfort improvement.

The idea is not completely new: both industry and academy have explored some applications of active aerodynamic surfaces. Prof. Savkoor has published a series of papers pioneering the use of active aerodynamics surfaces in cars., focusing mainly on pitch control in Savkoor et al. (2001), and yaw rate control in Savkoor and Happel (1996). Automotive manufacturers implemented more basic, adaptive solutions. For example, the Pagani Huayra uses active spoilers to increase downforce during high speed braking.

This work focuses on designing an AAS control system to optimize comfort without affecting road-holding. Vertical dynamics is usually influenced through suspensions. Suspensions generate an internal force which inevitably introduces a trade-off between ride comfort and vehicle handling. In this study, it will be shown that AAS control can alleviate this trade-off opening up space for a better tuning of the suspension (for both passive and semi-active suspension systems).

This work continues along prof. Savkoor's path extending his initial idea in two specific directions:

- the main focus of the present work is on ride comfort and the trade-off with road holding.
- A detailed mechatronics oriented analysis is carried out for several design parameters.

The paper is organized as follows. In Section 2 the problem is set-up recalling the main models; furthermore the main indexes and simulation protocols are defined. Section 3 focuses on the design of the controller. A loop shaping technique is adopted and several parameters are investigated to formalize the main design considerations that the practitioner has to consider when tuning the system. Section 4 analyzes the performance of the proposed system.

Corno et al. (2013) complements these results considering a different actuator configuration in the attempt of solely improving road-holding.

2. PRELIMINARIES AND MODELS

This section describes the system layout and recalls the simulation and design models; the main performance indexes and simulation protocols are defined. Figure 1 describes the system layout: a sport vehicle with four independent active airfoils. The airfoils are attached to the sprung mass and are servo-controlled. An accelerometer measures the sprung mass vertical acceleration.

2.1 Vehicle model

Two vehicle models are employed. The first model is a complete multi-body simulation model (Carsim). This model is too

Copyright © 2014 IFAC

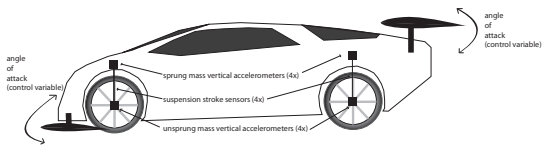

Fig. 1. System layout with actuator and sensors.

Table 1. Quarter car parameters

Symbol	Description	Value	Unit
M	Sprung mass	310	kg
m	Unsprung mass	40	kg
c	Damper stiffness	2500	Ns/m
k	Spring constant	$3{\cdot}10^4$	N/m
k_t	Tire equivalent spring constant	$2{\cdot}10^5$	N/m
ρ	Air density	1.275	kg/m^3

complex for control system design and it is used only for validation; a control-oriented model is needed for system design and analysis.

The quarter-car model Savaresi et al. (2010) (see Figure 2) well describes the vertical dynamics of interest. The classical model needs to be augmented to include the effect of the aerodynamic forces. To do so an input is added to the classic quarter car model:

$$\begin{cases} M\ddot{z}(t) = -c(\dot{z}(t) - \dot{z}_t(t)) - k(z(t) - z_t(t)) + F_{lift}(t) \\ m\ddot{z}_t(t) = c(\dot{z}(t) - \dot{z}_t(t)) + k(z(t) - z_t(t)) - k_t(z_t(t) - z_r(t)) \end{cases} \tag{1}$$

z, $\dot{z}$ and $\ddot{z}$ refer to the sprung mass vertical position, speed and acceleration, while z_t, $\dot{z}_t$ and $\ddot{z}_t$ are respectively the wheel center vertical position, speed and acceleration. The system has two inputs: the unmeasurable road height z_r and the partially controllable aerodynamic lift F_{lift}. k and c are respectively the stiffness and damping of the suspension. Table 1 summarizes the main vehicle parameters. System (1) defines four fundamental transfer functions:

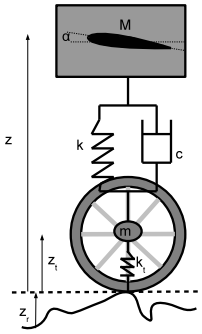

Fig. 2. Quarter car model.

$$G_1(s) = \frac{Z_{def_t}(s)}{F_{lift}(s)}, \qquad G_2(s) = \frac{s^2 Z(s)}{F_{lift}(s)}, \tag{2}$$

$$H_{1OL}(s) = \frac{Z_{def_t}(s)}{Z_r(s)}, \qquad H_{2OL}(s) = \frac{s^2 Z(s)}{Z_r(s)}. \tag{3}$$

The expressions in (3) are the well-known quarter car transfer functions from road height to tire deflection ($z_{def_t} = z - z_r$) and to vertical chassis acceleration. The transfer functions in (2) represent the effect of the controllable input; Figure 3 plots the Bode diagrams. In particular, $G_1(s)$ is the transfer function from the vertical aerodynamic force to tire deflection, and $G_2(s)$ is the transfer function from the lift force to chassis vertical acceleration. Note that in $G_1(s)$ both resonances are present; whereas in $G_2(s)$ only the body resonance is visible: the unsprung mass does not affect the external force dynamics to the chassis acceleration. Further, unsurprisingly, the dynamics from the lift force to the sprung mass has a higher gain than to the unsprung mass.

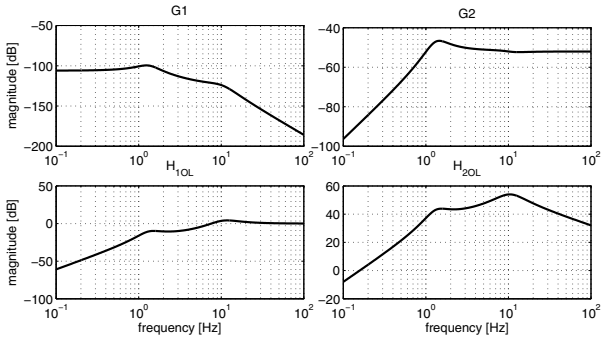

Fig. 3. Bode diagrams of the magnitude of the four main characteristic quarter-care transfer functions.

2.2 Aerodynamic actuator model

F_{lift} is not fully controllable, it depends on the airfoil properties and the vehicle velocity. The airfoil generates lift and drag forces and a pitching moment according to:

$$F_{lift} = \frac{1}{2}\rho V^2 S C_{lift}(\alpha) \qquad F_{drag} = \frac{1}{2}\rho V^2 S C_{drag}(\alpha)$$
$$M_{pitch} = \frac{1}{2}\rho V^2 S c_h C_{pitch}(\alpha) \tag{4}$$

where ρ is the air density, V is the air flow speed, S is the airfoil surface, c_h is the airfoil chord, α is the angle of attack. C_{lift}, C_{drag} and C_{pitch} are coefficients which, at steady state, depend on the Reynolds number, airfoil shape, roughness and the angle of attack (α) *i.e.* the angle between the airflow and the wing axis. The angle of attack is the actual control variable, as the wing is servo-actuated. Figure 4 plots the angle of attack dependency of the three coefficients of a NACA0014 airfoil Abbott et al. (1945). The lift coefficient is bounded.

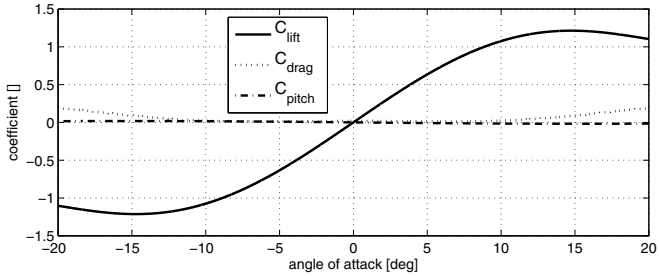

Fig. 4. Static Lift, drag and pitch coefficient as a function of the angle of attack.

The maximum lift force is generated at $\alpha = 15°$. Above that value, flow separation occurs. To avoid exceeding the airfoil stall point, the controlled angle of attack is constrained to the $[-15°, +15°]$ region.

Figure 4 shows the static coefficients. The aerodynamic force dynamics are modeled according to Jones' model (see Leish-

man (2006) for more details) by the following linear parameter varying system:

$$\begin{cases} \begin{bmatrix} \dot{x}_1(t) \\ \dot{x}_2(t) \end{bmatrix} = \dfrac{2V}{c} \begin{bmatrix} -b_1 & 0 \\ 0 & -b_2 \end{bmatrix} \begin{bmatrix} x_1(t) \\ x_2(t) \end{bmatrix} + \begin{bmatrix} 1 \\ 1 \end{bmatrix} \alpha(t) \\ C_{lift}(t) = C_{lift}^{static}(\alpha) \dfrac{2V}{c} \begin{bmatrix} A_1 b_1 & A_2 b_2 \end{bmatrix} \begin{bmatrix} x_1(t) \\ x_2(t) \end{bmatrix} \end{cases} \tag{5}$$

with $A_1 = 0.165$, $A_2 = 0.335$, $b_1 = 0.0455$, $b_2 = 0.3$.

The four AAS's are each actuated by a servo controller (see Panzani et al. (2013)). The servo control inverts the lift coefficient characteristics, effectively linearizing the airfoil characteristic within its maximum and minimum lift coefficient. The airfoils is thus considered to be controlled in lift coefficient. The servo-mechanism has a 10Hz bandwidth.

2.3 Road Profile

Two kinds of experiments are considered: sine-sweep tests and more realistic road profile simulations. Sine-sweep tests are generated by a multi-tone sinusoidal road height excitation with a decreasing amplitude. Although not realistic, sine sweep tests are very useful to provide a frequency-domain analysis of the performance. The final validation is done on more realistic road profiles. They are generated by the a filtered white noise profile. The variance of the white noise is tuned according to the International Roughness Index (IRI) standard Paterson (1986). The IRI is a dimensionless number which measures the road profile roughness: $IRI = 0$ m/km implies a perfectly flat road, while higher IRI values refer to rougher road profiles.

2.4 Performance Indexes

Two main performance criteria are defined: the comfort-oriented index and the road-holding oriented index. The comfort oriented index, J_C, evaluates the vertical acceleration the vehicle occupants are subject to. It is determined by:

$$J_C = \frac{\mathscr{C}(F_c, 0, 20Hz)}{\mathscr{C}(F_c^{nom}, 0, 20Hz)} \qquad F_c(f) = \frac{G_{\ddot{z}_f}(f)}{G_{\ddot{z}_r}(f)} \tag{6}$$

where $G_{\ddot{z}}(f)$ and $G_{\ddot{z}_r}(f)$ are the power spectral densities of the chassis filtered vertical acceleration and of the road vertical acceleration. The function $\mathscr{C} : \mathbb{R} \times \mathbb{R} \times \mathbb{R} \to \mathbb{R}$ is:

$$\mathscr{C}(X, \underline{f}, \overline{f}) = \int_{\underline{f}}^{\overline{f}} |X(f)|^2 \, \mathrm{d}f. \tag{7}$$

The sprung mass acceleration is filtered through a shaping filter that enhances the frequency range ([3, 10] Hz) where the human body is most sensitive to vibrations. It is defined by the ISO-2631-1.

Conversely, road holding is evaluated by considering the tire deflection

$$J_{RH} = \frac{\mathscr{C}(F_{z_{def_t}}, 0, 20Hz)}{\mathscr{C}(F_{z_{def_t}}^{nom}, 0, 20Hz)} \qquad F_{z_{def_t}}(f) = \frac{G_{z_{def_t}}(f)}{G_{z_r}(f)}. \tag{8}$$

The above-defined indexes are useful to analyze the comfort road holding trade-off. Figure 5 plots the normalized performance diagram; each point has coordinates (J_C,J_{RH}) and it is related to a different quarter car configuration. In this example, the passive suspension curve (each point related to different passive damper stiffness) is noted. Observe that, by acting on suspension parameters, it is impossible to increase road holding without affecting comfort Savaresi et al. (2010).

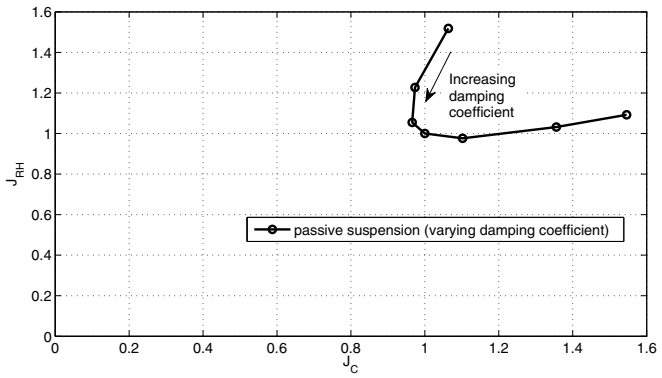

Fig. 5. Comfort - Road Holding Diagram. Curves related to passive suspensions with different damper tuning.

The remainder of the work will prove that the use of actively controlled aerodynamic surfaces can alleviate this trade-off; the lift force is an external force that acts directly on the chassis. Seen in the trade-off plane, this application aims at moving horizontally to the left, starting from the nominal passive suspension (1,1).

3. CONTROL SYSTEM DESIGN

Figure 3 shows a very direct dynamical connection between the lift force and the sprung mass dynamics; whereas the effect of the lift force on the unsprung mass is filtered. This naturally points to setting up the control problem as a comfort oriented problem.

To control the aerodynamic surfaces, four independent corner controllers are designed and tuned on the quarter car model. The control problem is formulated as a classical single input-single output problem. Figure 6 shows the block diagram of one corner. The scheme has four components. The controller

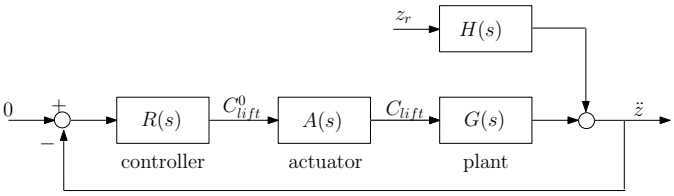

Fig. 6. Control system block diagram.

is designed to track a null chassis acceleration reference. It outputs the desired lift coefficient C_{lift}^0. The servo-mechanism $A(s)$ actuates the airfoil to track the desired lift coefficient. The actual lift C_{lift} drives the vehicle dynamics $G(s)$. The measured vertical chassis acceleration is the result of the lift coefficient and of the effect of the road through the dynamics $H(s)$.

The design of $R(s)$ is set as a loop shaping problem with the objective of achieving a good road disturbance rejection. Calling $L(s)$ the loop transfer function, the road disturbance properties are described by

$$F(s) = \frac{A(s)}{Z_r(s)} = \frac{H(s)}{1 + L(s)} \tag{9}$$

The controller $R(s)$ is designed so to impose a pass-band like behavior to $L(s)$:

$$R(s) = k \frac{\left(s^2 + 2\zeta\omega_n s + \omega_n^2\right)(s + z_1)}{(s + p_1)^2 (s + p_2)} \tag{10}$$

in this way the control action is focused on the frequency range of interest, avoiding both the high frequencies (where the model of the aerodynamic force breaks down and is not reliable) and the low frequency. Low frequencies are not critical from the comfort standpoint. If the controller tried to act at low frequency, it would quickly drive the airfoil to saturation, in the attempt of "flying" the car. Figure 7 plots the magnitude Bode plot of several possible tuning of the resulting loop transfer function. The frequency at which the L magnitude Bode diagram crosses 0 dB from above is loosely referred to as the control bandwidth and parametrizes the controller. The

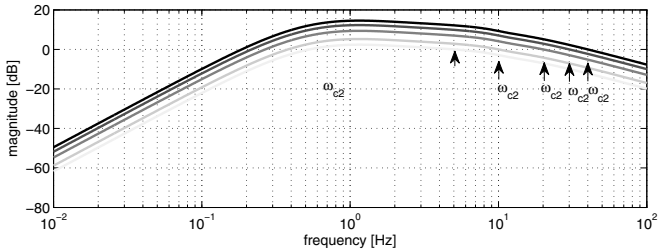

Fig. 7. Loop transfer function ($L(s)$) magnitude Bode diagram for different possible tunings.

higher the gain is in the pass band region and the wider the bass band region is, the better disturbance rejection is obtained. However there will be limitations due to the capability of the airfoil to generate the desired forces. Different factors need to be considered when tuning the controller. In the following a sequential tuning procedure is adopted; at first the performance bound considering an ideal actuator is assessed as a proof of concept; afterwards the tuning is refined considering a realistic actuator in terms of bandwidth and force that it can deliver.

3.1 Controller tuning

Let us consider a controller with a bandwidth of 40 Hz and, for now, remove all saturations. In this ideal set-up the airfoil is capable of generating any desired force.

Figure 8 plots the trade-off diagram comparing several passive tuning and the performance obtained with the 40 Hz controller combined with the nominal passive tuning suspension. The data are simulated using the sine sweep experiment. The plot

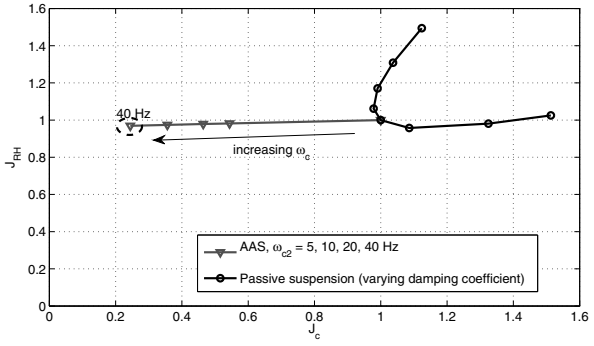

Fig. 8. Comfort - Road Holding Diagram. Comparison of passive suspension

shows that the rationale of comfort oriented AAS control holds. The control scheme horizontally translates the performance, improving the comfort index without negatively affecting road holding. The 80% improvement figure is to be considered an ideal upper bound.

A 40 Hz controller bandwidth is not achievable for technological reasons: the actuator would require too much power. Furthermore at those frequency the airfoil model looses validity because of turbulence. It is therefore important to assess the effects of reducing the controller bandwidth on the performance. Figure 8 also plots the comfort road holding trade-off results for lower bandwidth. As expected, the performance improvement decreases; a slower control scales the comfort index gain without negatively affecting the road holding index. The controller bandwidth tuning is therefore simplified, as no negative effects arise from a slower controller. This analysis is better understood considering the comfort and road-holding variables power spectra separately. Figure 9 plots the numerically evaluated frequency response from road disturbance to chassis acceleration and to tyre deflection. As expected, the

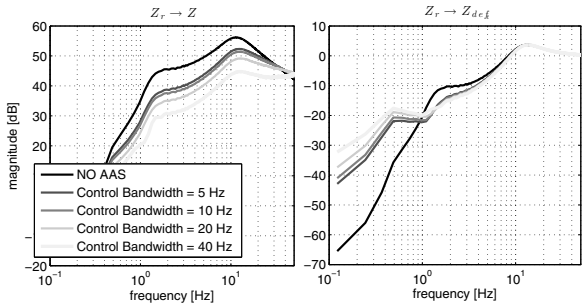

Fig. 9. Experimental frequency response for different controller bandwidth.

chassis acceleration gain is reduced in the desired bandwidth; whereas outside the bandwidth the dynamics is not negatively affected. The analysis is somewhat more convolute for the tyre deformation variable. There is a trade-off between low $f < 1$ Hz) and high ($f > 1$ Hz) frequency. At low frequency the AAS controller negatively affects the transfer function gain. At high frequency the effect is beneficial. Figure 3 provides an interpretation of this; the response from the lift force to the tyre deformation is a low pass filter with a cut-off frequency of around 1 Hz; when a low frequency force is applied on the chassis, it is transferred to the tyre affecting its load. As the frequency increases, this effect is filtered out. This effect is not visible in the overall trade-off map because the absolute gain of the transfer function below 1 Hz is considerably lower than above 1 Hz. In the overall road-holding economy, the low frequency tyre deformation contribution is negligible.

The controller bandwidth has a major influence on the actuator power requirements. Figure 10 plots the comfort index required actuator power trade-off. To improve the plot readability, the power is normalized [1] with respect to the worst case scenario. From figure, one notices that the trade-off is non linear. A bandwidth of 5 Hz represents a reasonable trade-off between the performance loss and the reduction of power with respect to the 40 Hz case. A 5 Hz bandwidth is also compatible with the servo bandwidth and Jones' fluid dynamics model.

Now that the effect of reducing the bandwidth down to a realistic value have been assessed; the second non-ideality is introduced, namely the airfoil characteristics. As seen in Figure

[1] as at this stage the airfoil size is not yet considered, the actual power value would not be meaningful.

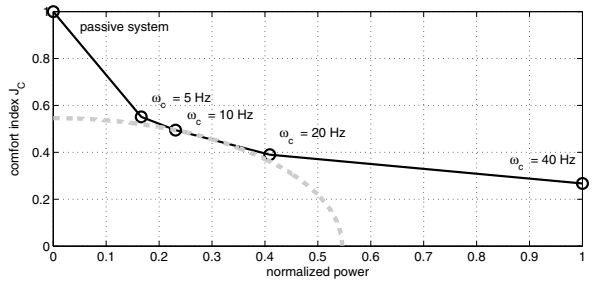

Fig. 10. Comfort index versus required normalized actuator power as function of control bandwidth.

4 and equations (4) the maximum force exertable by an airfoil is limited by its lift characteristic, the velocity (an uncontrollable time-varying parameter) and the airfoil surface. The wider the surface, the higher force the wing exerts. The maximum surface that can be used is limited by encumbrance considerations. The surface of the wing introduces a nonlinearity in the control system in the shape of a saturation: this may introduce negative effects and unwanted loss of performance.

To assess the loss of performance introduced by these non-idealities, several simulations have been run for different values of the airfoil surfaces on the quarter-car model at 200 km/h on the sine-sweep test. In this case, all the nonlinearities have been accounted for and modeled: servo dynamics, aerodynamics and nonlinear airfoil characteristics. Figure 11 plots the saturation rate during the simulation run, meaning the time spent in saturation with respect to the total time of the run. From the

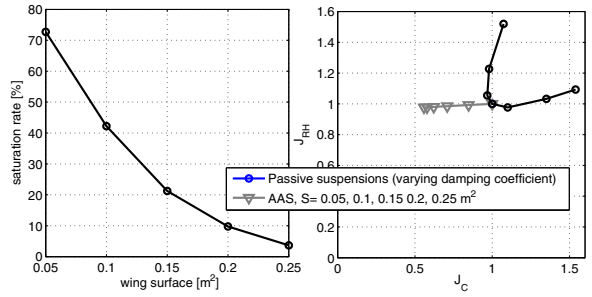

Fig. 11. Saturation rate (left) and comfort road holding map as a function of airfoil surface.

figure, it is immediately clear that, as the airfoil gets smaller, the actuator saturates more and more, basically behaving as a bang-bang controller. Figure 11 also plots the familiar trade-off map; a few considerations can be drawn:

- the airfoil size has a considerable effect on the overall performance.
- The performance gain is nonlinear. The first 0.05 m^2 gives the biggest relative gain in terms of performance. The relative gain improvement is then reduced for each additional 0.05 m^2.
- The nonlinearity does not affect the trade-off in a negative way. As the surface gets smaller, the performance decreases, but no unwanted interference with road holding is generated.

The nonlinearity does not undermine the main rationale: AAS control is capable of improving comfort without negatively affecting road-holding. This very fact makes the design of the airfoils relatively simple: "use the biggest airfoil that fits and that can be actuated". In the remainder of the paper, four airfoils of 0.15 m^2 are considered. This represents a reasonable trade-off between the size of the actuator and the performance. Depending on the vehicle and design considerations, the sizing could change and possibly also differentiated front to rear.

The section is concluded by a time domain representation of the performance obtained for different airfoils surfaces. Figure

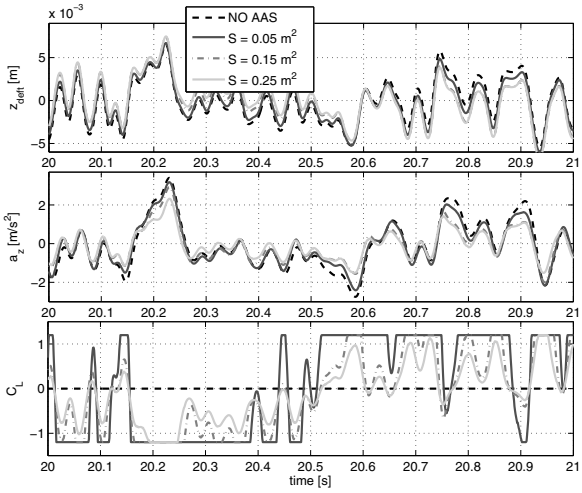

Fig. 12. Chassis vertical acceleration, tyre deflection and actuation for a sine sweep run at 200 km/h.

12 plots the chassis vertical acceleration, tyre deflection and reference C_{lift} for a run on a IRI 3.5 m/km road a run at 200 km/h. The plots show the effectiveness of the proposed control strategy. Note that the active aerodynamic surface is capable of reducing the sprung mass acceleration peaks.

In the following section a more detailed analysis of performances in realistic driving scenario is presented.

4. PERFORMANCE ANALYSIS

The performance and sensitivity analyses are carried out on the quarter car model with the control system designed in the previous section. The analysis addresses two important aspects: actuation power and velocity sensitivity. The analysis focused on straight running.

4.1 Power consumption

For each corner the actuation power is given by the sum of two terms: the inertial power (the power required to accelerate the airfoil) and the aerodynamic power (the power needed to overcome the pitching moment generated by the airfoil). Figure 13 plots the required power by a single corner for a 60 seconds run on a realistic surface with a IRI of 3.5 at 200 km/h. The power requirements are not negligible: the peak power is 1000 W (reached only instantaneously) and the required RMS power is 150 W. Although not negligible, this level of performance is achievable by state-of-the-art servo-motors.

4.2 Velocity sensitivity

The effect of driving velocity is investigated. The system is thought for fast moving sport vehicles and the effectiveness of the approach heavily depends on the vehicle velocity. Figure 14

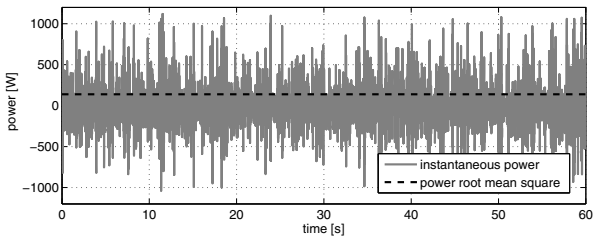

Fig. 13. Required actuation power for a single corner at 200 km/h on a IRI 3.5 road.

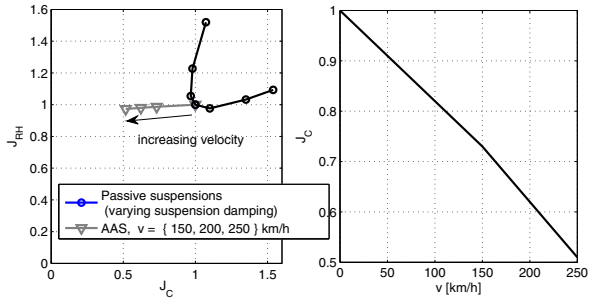

Fig. 14. Comfort-road holding trade-of (left) and J_C (rigth) as a function of velocity

plots the trade-off map as the velocity changes. The nominal system is driven on a 3.5 IRI road at different speeds ranging up to 250 km/h. The results are shown in Figure 14. The loss of performance is linear with the vehicle velocity, this may seem to contradict the quadratic nature of the dependency of the forces on airflow velocity. However recall that the maximum exertable force excites a saturation which has a inherent nonlinear effect. Notice, one more time, that the loss of performance in comfort is not associated to a loss of performance in road holding. The control of the AAS once again decouples the two aspects.

4.3 Complete vehicle model validation

Previously the tuning and performance of the AAS system have been discussed focusing on a single corner. Figure 15 shows the trade off maps of the complete multi-body case at 200 km/h on a IRI 3.5 road. The indexes are computed for the four corners. Simulations on the complete model confirm the analysis carried out on the single corner.

5. CONCLUSIONS

In this work a comfort-oriented ride-control using active aerodynamic surfaces has been presented. The control system minimizes the sprung mass oscillations by acting on four independent aerodynamic surfaces; as such it uses a genuinely closed-loop approach. The closed-loop approach enables the solution of the daunting comfort-road holding trade off that arises in suspension control.

A model-based controller is designed on the classical quarter car model; the proposed design and the several trade-offs involved in the tuning are discussed considering several parameters. Simulation validation shows that at high speed on average the use of AAS yields an improvement of 30% of the comfort performance without affecting road holding. The performance improvement comes at the cost of power requirements and a complex mechatronic design.

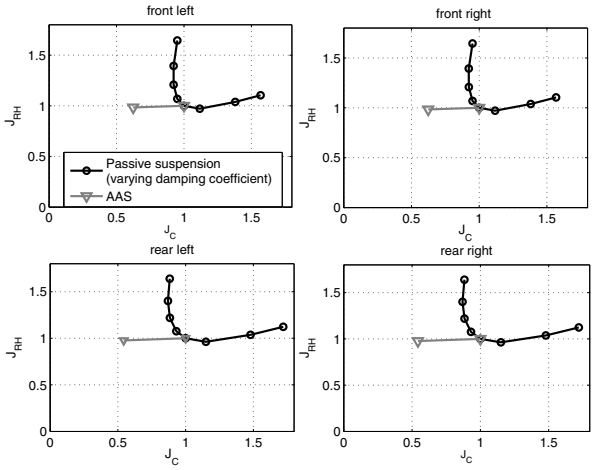

Fig. 15. Four corners comfort-road holding trade-off of the multi-body simulation.

REFERENCES

Abbott, I., Von Doenhoff, A., and Stivers Jr, L. (1945). Summary of airfoil data. Technical report.

Corno, M., Bottelli, S., Panzani, G., Tanelli, M., Spelta, C., and Savaresi, S. (2013). Improving high speed road-holding using actively controlled aerodynamic surfaces. In *Proceedings of the European Control Conference*, 1493 – 1498.

Corno, M., Gerard, M., Verhaegen, M., and Holweg, E. (2012). Hybrid abs control using force measurement. *IEEE Transactions on Control Systems Technology*, 20(5), 1223–1235.

Hong, K., Sohn, H., and Hedrick, J. (2002). Modified skyhook control of semi-active suspensions: a new model, gain scheduling, and hardware-in-the-loop tuning. *Journal of Dynamic Systems, Measurement, and Control*, 124(1), 158–167.

Leishman, J. (2006). *Principles of helicopter aerodynamics*. Cambridge Univ Pr.

Panzani, G., Corno, M., and Savaresi, S.M. (2013). On adaptive electronic throttle control for sport motorcycles. *Control Engineering Practice*, 21(1), 42–53.

Paterson, W. (1986). International roughness index: Relationship to other measures of roughness and riding quality. *Transportation Research Record*, (1084).

Savaresi, S., Poussot-Vassal, C., Spelta, C., Sename, O., and Dugard, L. (2010). *Semi-active Suspension Control Design for Vehicles*. Elsevier (Butterworth-Heinemann), Oxford, UK.

Savkoor, A. and Happel, H. (1996). Aerodynamic vehicle ride control with active spoilers. In *Proceedings of International Symposium on Advanced Vehicle Control*, 647–682.

Savkoor, A., Manders, S., and Riva, P. (2001). Design of actively controlled aerodynamic devices for reducing pitch and heave of truck cabins. *JSAE review*, 22(4), 421–434.

Todeschini, F., Corno, M., Panzani, G., and Savaresi, S.M. (2014). Adaptive position-pressure control of a brake by wire actuator for sport motorcycles. *European Journal of Control*, 20(2), 79 – 86.